



Light vector meson production in pp collisions at $\sqrt{s} = 7$ TeV[☆]

ALICE Collaboration

ARTICLE INFO

Article history:

Received 17 December 2011
 Received in revised form 15 March 2012
 Accepted 15 March 2012
 Available online 19 March 2012
 Editor: L. Rolandi

ABSTRACT

The ALICE experiment has measured low-mass dimuon production in pp collisions at $\sqrt{s} = 7$ TeV in the dimuon rapidity region $2.5 < y < 4$. The observed dimuon mass spectrum is described as a superposition of resonance decays ($\eta, \rho, \omega, \eta', \phi$) into muons and semi-leptonic decays of charmed mesons. The measured production cross sections for ω and ϕ are $\sigma_\omega(1 < p_t < 5 \text{ GeV}/c, 2.5 < y < 4) = 5.28 \pm 0.54(\text{stat}) \pm 0.49(\text{syst}) \text{ mb}$ and $\sigma_\phi(1 < p_t < 5 \text{ GeV}/c, 2.5 < y < 4) = 0.940 \pm 0.084(\text{stat}) \pm 0.076(\text{syst}) \text{ mb}$. The differential cross sections $d^2\sigma/dy dp_t$ are extracted as a function of p_t for ω and ϕ . The ratio between the ρ and ω cross section is obtained. Results for the ϕ are compared with other measurements at the same energy and with predictions by models.

© 2012 CERN. Published by Elsevier B.V. Open access under CC BY-NC-ND license.

1. Introduction

The measurement of light vector meson production (ρ, ω, ϕ) in pp collisions provides insight into soft Quantum Chromodynamics (QCD) processes in the LHC energy range. Calculations in this regime are based on QCD inspired phenomenological models [1] that must be tuned to the data, in particular for hadrons that contain the u, d, s quarks. The evolution of particle production as a function of \sqrt{s} is difficult to establish. Measurements at mid-rapidity in pp collisions at the beam injection energy of the LHC ($\sqrt{s} = 0.9$ TeV) were performed by the ALICE experiment [2], and compared with several PYTHIA [3] tunes and PHOJET [4]. The comparison showed that, for transverse momenta larger than ~ 1 GeV/c, the strange particle spectra are strongly underestimated by the models, by a factor of 2 for K_S^0 and 3 for hyperons, with a smaller discrepancy for the ϕ . Extending the measurements to larger energies and complementary rapidity domains is needed in order to further constrain the models.

Moreover, light vector meson production provides a reference for high-energy heavy-ion collisions. In fact, key information on the hot and dense state of strongly interacting matter produced in these collisions can be extracted measuring light meson production [5–13].

The ALICE experiment at the LHC can access vector mesons produced in the rapidity range $2.5 < y < 4$ through their decays into muon pairs.¹ In this Letter we report results obtained in pp collisions at $\sqrt{s} = 7$ TeV in the dimuon transverse momentum range

$1 < p_t < 5$ GeV/c based on the full data sample collected in 2010 with a muon trigger with no p_t selection. The measurement is done via a combined fit of the dimuon invariant mass spectrum after combinatorial background subtraction.

2. Experimental setup

The ALICE detector is fully described elsewhere [14]. The main detectors relevant for this analysis are the forward muon spectrometer, which covers the pseudo-rapidity region $-4 < \eta < -2.5$, the VZERO detector and the Silicon Pixel Detector (SPD) of the Inner Tracking System.

The elements of the muon spectrometer are a front hadron absorber, followed by a set of tracking stations, a dipole magnet, an iron wall acting as muon filter and a trigger system.

The front hadron absorber is made of carbon, concrete and steel and is placed at a distance of 0.9 m from the nominal interaction point (IP). Its total length of material corresponds to ten hadronic interaction lengths. The dipole magnet is 5 m long and provides a magnetic field of up to 0.7 T in the vertical direction which gives a field integral of 3 Tm.

The muon tracking is provided by a set of five tracking stations, each one composed of two cathode pad chambers. The stations are located between 5.2 and 14.4 m from the IP, the first two upstream of the dipole magnet, the third in the middle of the dipole magnet gap and the last two downstream. The intrinsic spatial resolution of the tracking chambers is ~ 100 μm in the bending direction.

A 1.2 m thick iron wall, corresponding to 7.2 hadronic interaction lengths, is placed between the tracking and trigger systems and absorbs the residual secondary hadrons emerging from the front absorber. The front absorber together with the muon filter stops muons with momentum lower than 4 GeV/c. The muon trigger system consists of two detector stations, placed at 16.1 and

[☆] © CERN for the benefit of the ALICE Collaboration.

¹ In the ALICE coordinates, the muon spectrometer covers the pseudo-rapidity range $-4 < \eta < -2.5$, where the z axis is oriented along the beam direction, anti-clockwise. However, since in pp collisions results are symmetric with respect to $y = 0$, we prefer to drop the negative sign when quoting the rapidity values.

17.1 m from the IP. Each one is composed of two planes of resistive plate chambers (RPC), with a time resolution of about 2 ns.

The SPD consists of two cylindrical layers of silicon pixel detectors, positioned at a radius of 3.9 and 7.6 cm from the beam. The pseudo-rapidity range covered by the inner and the outer layer is $|\eta| < 2.0$ and $|\eta| < 1.4$, respectively. Besides contributing to the primary vertex determination, it is used for the input of the level-0 trigger (L0).

The VZERO detector consists of two arrays of plastic scintillators placed at 3.4 m and -0.9 m from the IP and covering the pseudo-rapidity regions $2.8 < \eta < 5.1$ and $-3.7 < \eta < -1.7$, respectively. This detector provides timing information for the L0 trigger and has a time resolution better than 1 ns, thus giving the possibility to reject beam-halo and beam-gas interactions in the off-line analysis.

3. Data selection and analysis

During the pp run in 2010, the instantaneous luminosity delivered by the LHC to ALICE ranged from 0.6×10^{29} to $1.2 \times 10^{30} \text{ cm}^{-2} \text{ s}^{-1}$. The fraction of events with multiple interactions in a single bunch crossing was less than 5%. The data sample used in this analysis was collected using a single-muon trigger, which is activated when at least three of the four RPC planes in the two muon trigger stations give a signal compatible with a track in the muon trigger system. To evaluate the integrated luminosity (\mathcal{L}_{int}), another sample was collected in parallel using a minimum bias (MB) trigger, independent of the muon trigger. It is activated when at least one out of the 1200 SPD readout chips detects a hit or when at least one of the two VZERO scintillator arrays has fired, in coincidence with the arrival of bunches from both sides.

The integrated luminosity was determined by measuring the MB cross section σ_{MB} and counting the number of MB events. The σ_{MB} value is 62.3 mb, and is affected by a 3.5% systematic uncertainty. It was obtained measuring the cross section σ_{VOAND} [15], for the occurrence of coincident signals in the two VZERO detectors (VOAND) in a van der Meer scan [16]. The factor $\sigma_{\text{VOAND}}/\sigma_{\text{MB}}$ was obtained as the fraction of MB events where the L0 trigger input corresponding to the VOAND condition has fired. Its value is 0.87 and is stable within 0.5% over the analysed data. The full data sample used for this analysis was used to extract the ω and ϕ p_t distributions. Part of the data was not collected with the MB trigger in parallel with the muon trigger. For this fraction, the integrated luminosity could not be measured and the ω and ϕ cross sections were determined with the remaining sub-sample corresponding to $\mathcal{L}_{\text{int}} = 55.7 \text{ nb}^{-1}$. A rough estimation based on the number of muon triggers taken in this sub-sample and in the full data set gives an integrated luminosity of approximately 85 nb^{-1} for the latter.

Track reconstruction in the muon spectrometer is based on a Kalman filter algorithm [17,18]. Straight line segments are formed from the clusters on the two planes of each of the most downstream tracking stations (4 and 5), since these are less affected by the background coming from soft particles that emerge from the front absorber. Track properties are first estimated assuming that tracks originate from the IP and are bent in a uniform magnetic field in the dipole. Afterwards, track candidates starting in station 4 are extrapolated to station 5, or vice versa, and paired with at least one cluster on the basis of a χ^2 cut. Parameters are then recalculated using the Kalman filter. The same procedure is applied to the upstream stations, rejecting track candidates that cannot be matched to a cluster in the acceptance of the spectrometer. Finally, fake tracks that share the same cluster with other tracks are removed and a correction for energy loss and multiple Coulomb scattering in the absorber is applied by using the Branson correc-

tion [17]. The relative momentum resolution of the reconstructed tracks is 1% at 13 GeV/c, corresponding to the average momentum of muons coming from the ϕ decay.

Muons were selected requiring that the direction and position of each muon track reconstructed in the tracking chambers match the ones of the corresponding track in the trigger stations. A cut on the muon rapidity $2.5 < y_\mu < 4$ was applied in order to remove the tracks close to the acceptance borders. Muon pairs, obtained combining the muons in each event, were selected requiring that both muons satisfy these cuts. Approximately 291,000 opposite-sign (N_{+-}) and 197,000 like-sign (N_{++}, N_{--}) muon pairs passed these selections.

The opposite-sign pairs are composed of correlated and uncorrelated pairs. The former constitute the signal, while the latter, coming mainly from decays of pions and kaons into muons, form the combinatorial background, which was evaluated using an event mixing technique. Pairs were formed using reconstructed tracks, selected with the criteria described above, and coming from different events that contain a single track in the muon spectrometer. The distribution obtained was normalized to $2R\sqrt{N_{++}N_{--}}$, where N_{++} (N_{--}) is the number of like-sign positive (negative) pairs integrated in the full mass range. It is assumed that the like-sign pairs are uncorrelated. The fraction of correlated like-sign pairs, coming from the decay chain of beauty mesons and $B - \bar{B}$ oscillations [19] was determined from the measured open charm content and the ratio between open beauty and charm (see below). It amounts to $\approx 0.5\%$ for $1 < p_t < 5 \text{ GeV}/c$ and $M < 1.5 \text{ GeV}/c^2$, and was thus neglected. The R factor is defined as $A_{+-}/\sqrt{A_{++}A_{--}}$, where A_{+-} (A_{++}, A_{--}) is the acceptance for a $(+, -)$ ($(++, - -)$) pair, and takes into account possible correlations introduced by the detector. It was evaluated using two methods. The first employs MC simulations to determine the acceptances $A_{\pm\pm}$. The other method uses the mixed-event pairs to estimate R as $R = N_{+-}^{\text{mixed}}/2\sqrt{N_{++}^{\text{mixed}}N_{--}^{\text{mixed}}}$, where $N_{\pm\pm}^{\text{mixed}}$ is the number of mixed pairs for a given charge combination. The two methods are in agreement for $p_t > 1 \text{ GeV}/c$. We obtain $R = 0.95$ for $1 < p_t < 5 \text{ GeV}/c$. The event mixing procedure was cross-checked by comparing the results obtained for like-sign mixed pairs with the non-mixed ones. The shapes are identical, while the number of like-sign pairs estimated with the event mixing is lower than the one in the data by 5%. We take this value as the systematic uncertainty on the background normalization. The signal-to-background ratio for $1 < p_t < 5 \text{ GeV}/c$ is about 1 at the ϕ and ω masses. Alternatively, the combinatorial background can be evaluated using only the like-sign pairs in the non-mixed data, and calculating for each ΔM mass bin the quantity $2R(\Delta M)\sqrt{N_{++}(\Delta M)N_{--}(\Delta M)}$. Fig. 1 shows the invariant mass spectrum for opposite-sign muon pairs in different p_t ranges, together with the combinatorial background estimated with the event mixing technique or using the like-sign pairs. It is seen that the two techniques are in good agreement for $1 < p_t < 5 \text{ GeV}/c$. For lower pair transverse momenta both methods fail in describing the background. In this region, the method based on the like-sign pairs gives a background mass spectrum that overshoots the opposite-sign pair spectrum, while the event mixing technique does not reproduce the non-mixed like-sign pairs spectra. The analysis is thus limited to $1 < p_t < 5 \text{ GeV}/c$. The event mixing technique is used, since it is less affected by statistical fluctuations.

After subtracting the combinatorial background from the opposite-sign mass spectrum, we obtain the raw signal mass spectrum shown in Fig. 2. The mass resolution at the ϕ mass is $\sigma_M \approx 60 \text{ MeV}/c^2$, in good agreement with the Monte Carlo simulation. The processes contributing to the dimuon mass spectrum are the light meson ($\eta, \rho, \omega, \eta', \phi$) decays into muons and the

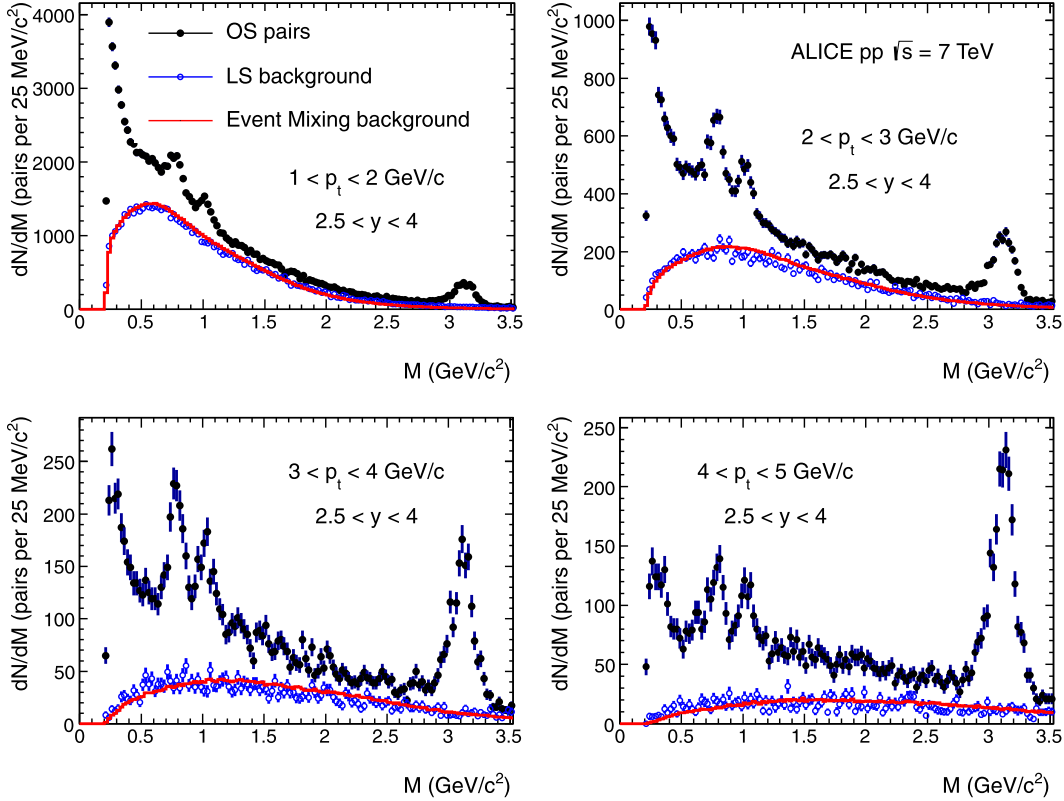


Fig. 1. (Colour online.) Invariant mass spectra for opposite-sign muon pairs in pp at $\sqrt{s} = 7$ TeV in different p_t ranges. The combinatorial background, evaluated from opposite-sign pairs in mixed events (red line) or like-sign pairs in non-mixed events (blue points), is also shown.

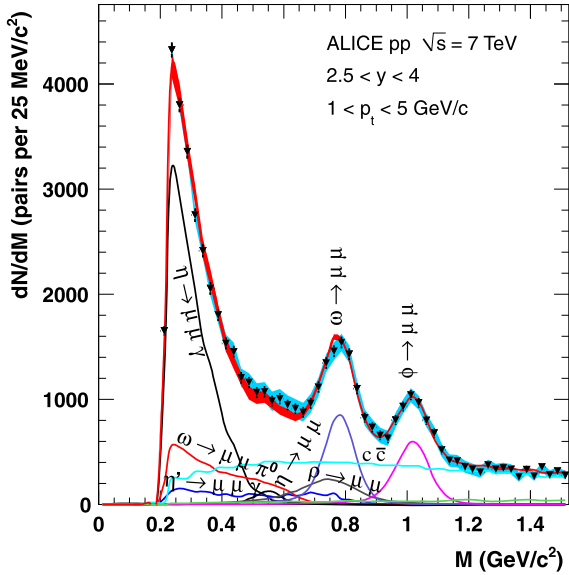


Fig. 2. (Colour online.) Dimuon invariant mass spectrum in pp at $\sqrt{s} = 7$ TeV after combinatorial background subtraction for $1 < p_t < 5$ GeV/c (triangles). Light blue band: systematic uncertainty from background subtraction. Red band: sum of all simulated contributions. The width of the red band represents the uncertainty on the relative normalization of the sources.

correlated semi-leptonic open charm and beauty decays. The light meson contributions were obtained performing a simulation based on a hadronic cocktail generator. The input rapidity distributions for all particles are based on a parametrization of PYTHIA 6.4 [3] results obtained with the Perugia-0 tune [20]. The same proce-

dure is followed for the η' p_t distribution, while for ρ , ω and ϕ the transverse momentum is described with a power-law function, used also by the HERA-B experiment to fit the ϕ p_t^2 spectrum [21]:

$$\frac{dN}{dp_t} = C \frac{p_t}{[1 + (p_t/p_0)^2]^n}. \quad (1)$$

The parameters n and p_0 were tuned iteratively to the results of this analysis. The p_t distribution of η is based on preliminary results from η production yields measured in the two-photon decay channel by ALICE [22]. The open charm and beauty generation is based on a parametrization of PYTHIA [17]. The detector response for all these processes is obtained with a simulation that uses the GEANT3 [23] transport code. The simulation results are then subjected to the same reconstruction and selection chain as the real data. The invariant mass spectrum is fitted with a superposition of the aforementioned contributions. The free parameters of the fit are the normalizations of the $\eta \rightarrow \mu\mu\gamma$, $\omega \rightarrow \mu\mu$, $\phi \rightarrow \mu\mu$ and open charm signals. The processes $\eta \rightarrow \mu\mu$ and $\omega \rightarrow \mu\mu\pi^0$ are fixed according to the relative branching ratios. The contribution from $\rho \rightarrow \mu\mu$ was fixed by the assumption that the production cross section of ρ and ω are equal [24–26]. The η' contribution was set fixing the ratio between the η' and η cross sections according to PYTHIA. The ratio between the open beauty and open charm was fixed according to the results from the LHCb Collaboration [27,28]. The main sources of systematic uncertainty are the background normalization and the relative normalization of the sources, mainly due to the error on the branching ratios for the ω and η' Dalitz decays. The raw numbers of ϕ and $\rho + \omega$ resonances obtained from the fit are $N_{\phi}^{\text{raw}} = (3.20 \pm 0.15) \times 10^3$ and $N_{\rho+\omega}^{\text{raw}} = (6.83 \pm 0.15) \times 10^3$.

4. Results

The ϕ production cross section was evaluated in the range $2.5 < y < 4$, $1 < p_t < 5$ GeV/c through the formula:

$$\sigma_\phi = \frac{N_\phi^{\text{raw}}}{A_\phi \varepsilon_\phi \text{BR}(\phi \rightarrow l^+l^-)} \frac{\sigma_{\text{MB}}}{N_{\text{MB}}} \frac{N_\mu^{\text{MB}}}{N_\mu^{\mu-\text{MB}}},$$

where N_ϕ^{raw} is the measured number of ϕ mesons, A_ϕ and ε_ϕ are the geometrical acceptance and the efficiency respectively, N_{MB} is the number of minimum bias collisions, σ_{MB} is the ALICE minimum bias cross section in pp collisions at $\sqrt{s} = 7$ TeV, and $N_\mu^{\text{MB}}/N_\mu^{\mu-\text{MB}}$ is the ratio between the number of single muons collected with the minimum bias trigger and with the muon trigger in the region $2.5 < y_\mu < 4$, $p_t^\mu > 1$ GeV/c. The number of minimum bias collisions was corrected, as a function of time, by the probability to have multiple interactions in a single bunch crossing. Finally, $\text{BR}(\phi \rightarrow l^+l^-) = (2.95 \pm 0.03) \times 10^{-4}$ is the branching ratio into lepton pairs. Assuming lepton universality, this number is obtained as a weighted mean of the measured branching ratio in $\mu^+\mu^-$ with that into e^+e^- , because the latter has a much smaller experimental uncertainty than the former [29]. The number of ϕ mesons was evaluated by performing a fit to the mass spectrum for each $\Delta p_t = 0.5$ GeV/c interval in the transverse momentum range covered by the analysis. The acceptance-corrected results were then summed in order to obtain the total number of ϕ mesons. In this way the dependence of the acceptance correction on the input p_t distribution used for the Monte Carlo simulation becomes insignificant. Alternatively, a fit was performed on the mass spectrum integrated over $1 < p_t < 5$ GeV/c and a global correction factor was applied. The results of the two approaches agree within 3%. The first approach was used for the results reported in this Letter. The ϕ meson acceptance and efficiency correction in the range covered by this analysis was evaluated through Monte Carlo simulations and ranges from 10% to 13%, depending on the data-taking period. The ratio $N_\mu^{\text{MB}}/N_\mu^{\mu-\text{MB}}$ strongly depends on the data taking conditions and was evaluated as a function of time.

We obtain $\sigma_\phi(1 < p_t < 5 \text{ GeV/c}, 2.5 < y < 4) = 0.940 \pm 0.084(\text{stat}) \pm 0.076(\text{syst}) \text{ mb}$. The systematic uncertainty results from the uncertainty on the ϕ branching ratio into dileptons (1%), the background subtraction (2%), the muon trigger and tracking efficiency (4% and 3% respectively), the minimum bias cross section (4%) and the ratio $N_\mu^{\text{MB}}/N_\mu^{\mu-\text{MB}}$ (3%). The first contribution has been described above. The uncertainty of the background normalization of 5% translates into a 2% systematic uncertainty on the cross section, which was evaluated by varying the normalization by $\pm 5\%$ and repeating the fit procedure on the resulting background subtracted spectra. Other contributions to the systematic uncertainty are common to all analyses in the dimuon channel, and are extensively discussed elsewhere [30]. Here, only the main points are briefly summarized. The muon trigger efficiency was estimated measuring the number of J/ψ mesons decaying into muons, after efficiency and acceptance corrections, in two ways: in the first case both muons were required to match the trigger, while in the second only one muon needed to fulfil this condition. The tracking efficiency was evaluated starting from the determination of the efficiency for individual chambers, computed by taking advantage from the redundancy of the tracking information in each station. The same procedure was applied to the data and to the Monte Carlo simulations. The differences in the results give the systematic uncertainty on the tracking efficiency. The error on the minimum bias cross section is mainly due to the uncertainties in the beam intensities [31] and in the analysis procedure adopted for the determination of the beam luminosity via the van der Meer scan. The error on the ratio $N_\mu^{\text{MB}}/N_\mu^{\mu-\text{MB}}$ was evaluated comparing the value

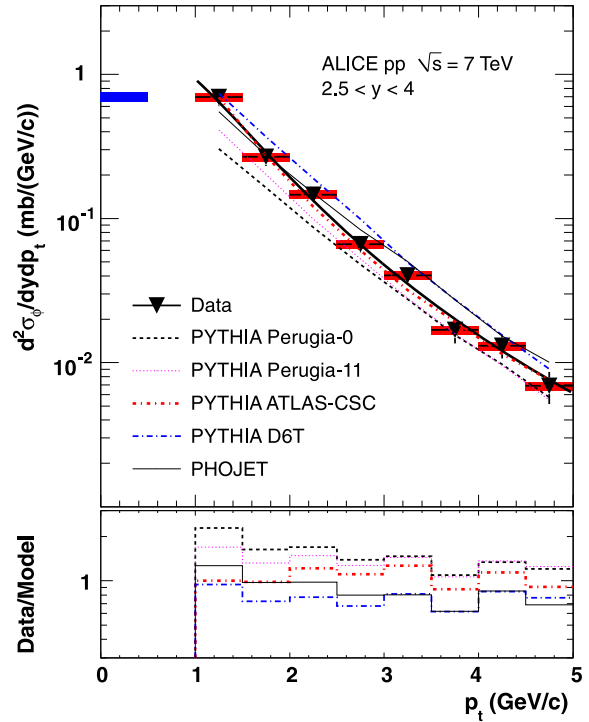


Fig. 3. Top: Inclusive differential ϕ production cross section $d^2\sigma_\phi/dydp_t$ for $2.5 < y < 4$. The error bars represent the quadratic sum of the statistical and systematic uncertainties, the red boxes the point-to-point uncorrelated systematic uncertainty, the blue box on the left the error on normalization. Data are fitted with Eq. (1) (solid line) and compared with the Perugia-0, Perugia-11, ATLAS-CSC and D6T PYTHIA tunes and with PHOJET. Bottom: Ratio between data and models.

measured as described above with the information obtained from the trigger scalers, taking into account the dead time of the triggers [32]. The uncertainty on the acceptance correction related to the limited knowledge of the rapidity distributions, was obtained changing the input distributions according to the models under test (see below). It resulted below 1% and was thus neglected. The uncertainty on the input p_t distribution in the Monte Carlo simulation is negligible, as discussed above. The uncertainty due to the unknown spin alignment of the ϕ was evaluated on the basis of the measurements reported in [10,33,34] and was found to be negligible.

Table 1 compares the present measurement with some commonly used tunes of PYTHIA [3] (Perugia-0 [20], Perugia-11 [35], ATLAS-CSC [36] and D6T [37]) and PHOJET [4]. It can be seen that Perugia-0 and Perugia-11 underestimate the ϕ cross section (by about a factor of 2 and 1.5, respectively), while the others agree with the measurement within its error.

The differential cross section $d^2\sigma_\phi/dydp_t$ is shown in Fig. 3 (top). Numerical values are reported in Table 2. p_t -dependent contributions to the systematic uncertainties, due to the uncertainty on trigger and tracking efficiency and background subtraction, are indicated as red boxes. The uncertainty on the minimum bias cross section, branching ratio and $N_\mu^{\text{MB}}/N_\mu^{\mu-\text{MB}}$ ratio contribute to the uncertainty in the overall normalization. As stated above, the ϕ cross section is extracted from a sub-sample of the data used to determine the p_t distribution, and is thus affected by a larger statistical uncertainty, resulting in a 5% contribution to the normalization error. Fitting the expression in Eq. (1) (solid line) to the differential cross section gives $p_0 = 1.16 \pm 0.23$ GeV/c and $n = 2.7 \pm 0.2$. The PYTHIA and PHOJET predictions are also displayed in Fig. 3, where the bottom panel shows the ratio between the measurement and the model predictions. PYTHIA with the

Table 1

Measured cross sections and ratios compared to the calculation from PYTHIA with several tunes and PHOJET in the range $1 < p_t < 5 \text{ GeV}/c$, $2.5 < y < 4$.

| | σ_ϕ (mb) | σ_ω (mb) | $\frac{N_\phi}{N_\rho + N_\omega}$ | $\sigma_\rho/\sigma_\omega$ |
|----------------------------|-----------------------------|--------------------------|------------------------------------|-----------------------------|
| ALICE $\mu\mu$ measurement | $0.940 \pm 0.084 \pm 0.076$ | $5.28 \pm 0.54 \pm 0.49$ | $0.416 \pm 0.032 \pm 0.004$ | $1.15 \pm 0.20 \pm 0.12$ |
| PYTHIA/Perugia-0 | 0.50 | 5.60 | 0.22 | 1.03 |
| PYTHIA/Perugia-11 | 0.62 | 7.81 | 0.20 | 1.03 |
| PYTHIA/ATLAS-CSC | 0.91 | 6.50 | 0.35 | 1.05 |
| PYTHIA/D6T | 1.12 | 9.15 | 0.30 | 1.04 |
| PHOJET | 0.87 | 6.89 | 0.30 | 1.08 |

Table 2

ϕ and ω differential cross sections for $2.5 < y < 4$. Statistical, bin-to-bin uncorrelated and correlated systematic errors are reported.

| p_t (GeV/c) | $d^2\sigma_\phi/dy dp_t$ (mb/(GeV/c)) | $d^2\sigma_\omega/dy dp_t$ (mb/(GeV/c)) |
|---------------|---|---|
| [1, 1.5] | $0.695 \pm 0.079 \pm 0.046 \pm 0.051$ | $3.69 \pm 0.35 \pm 0.24 \pm 0.31$ |
| [1.5, 2] | $0.268 \pm 0.032 \pm 0.018 \pm 0.020$ | $1.75 \pm 0.15 \pm 0.12 \pm 0.15$ |
| [2, 2.5] | $0.147 \pm 0.014 \pm 0.010 \pm 0.011$ | $0.857 \pm 0.069 \pm 0.057 \pm 0.073$ |
| [2.5, 3] | $0.0665 \pm 0.0074 \pm 0.0044 \pm 0.0049$ | $0.339 \pm 0.029 \pm 0.022 \pm 0.029$ |
| [3, 3.5] | $0.0403 \pm 0.0044 \pm 0.0027 \pm 0.0030$ | $0.220 \pm 0.019 \pm 0.011 \pm 0.019$ |
| [3.5, 4] | $0.0169 \pm 0.0031 \pm 0.0011 \pm 0.0012$ | $0.0880 \pm 0.0088 \pm 0.0058 \pm 0.0075$ |
| [4, 4.5] | $0.0131 \pm 0.0022 \pm 0.0009 \pm 0.0010$ | $0.0648 \pm 0.0062 \pm 0.0043 \pm 0.0055$ |
| [4.5, 5] | $0.0069 \pm 0.0017 \pm 0.0005 \pm 0.0005$ | $0.0301 \pm 0.0039 \pm 0.0020 \pm 0.0026$ |

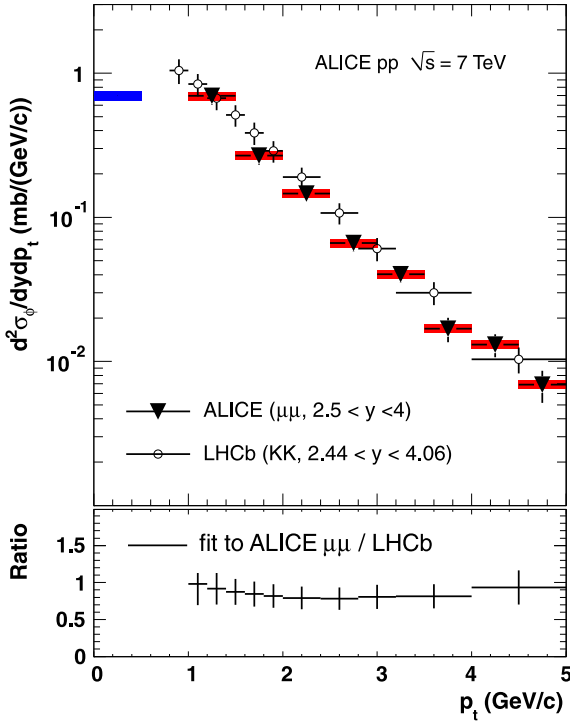


Fig. 4. (Colour online.) Top: Inclusive differential ϕ production cross section $d^2\sigma_\phi/dy dp_t$, as measured via the decay into dimuons (black triangles). The blue box on the left represents the error on normalization. The data are compared to the measurements in the kaon decay channel by LHCb (black open circles) [38]. Bottom: Fit to the differential cross section measured in dimuons divided by the cross section measured in the kaon channel by LHCb.

ATLAS-CSC and D6T tunes reproduce the measured differential cross section, while the others predict a slightly harder p_t spectrum.

The results are compared to measurements of $\phi \rightarrow K^+K^-$ for $2.44 < y < 4.06$ by the LHCb Collaboration [38] in Fig. 4. The observed shapes of the p_t distributions are similar. In order to compare with our integrated cross section result, the differential cross section measurement by LHCb was integrated for $1 < p_t < 5 \text{ GeV}/c$ and scaled by a small correction factor, obtained from PYTHIA (Perugia-0), to account for the slight difference in rapidity accep-

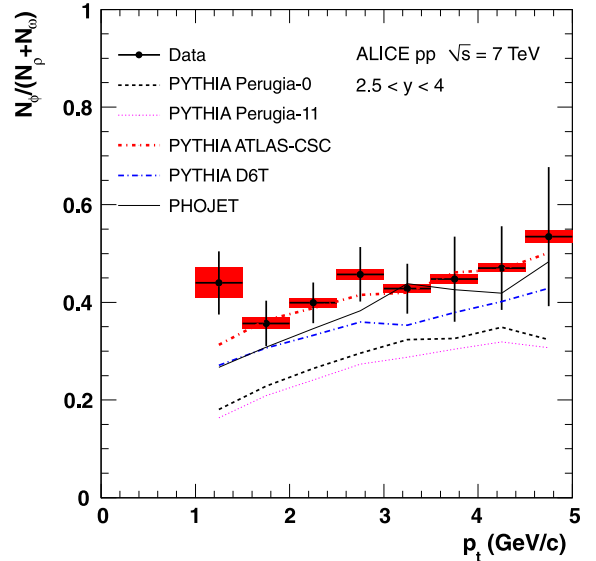


Fig. 5. Ratio $N_\phi/(N_\rho + N_\omega)$ as a function of the dimuon transverse momentum.

tance. The result is $\sigma_\phi = 1.07 \pm 0.15(\text{stat.} + \text{syst.}) \text{ mb}$. When the statistical errors and the part of the systematic uncertainty which is not correlated among the two experiments are properly taken into account, the two measurements are in agreement.

The ratio $N_\phi/(N_\rho + N_\omega) = BR(\phi \rightarrow \mu\mu)\sigma_\phi/[BR(\rho \rightarrow \mu\mu)\sigma_\rho + BR(\omega \rightarrow \mu\mu)\sigma_\omega]$, corrected for acceptance and efficiency, was calculated for $1 < p_t < 5 \text{ GeV}/c$, giving $0.416 \pm 0.032(\text{stat}) \pm 0.004(\text{syst})$. Systematic uncertainties are due to the normalizations of $\omega \rightarrow \mu\mu\pi^0$, $\eta' \rightarrow \mu\mu\gamma$ and combinatorial background. The uncertainty due to the acceptance and the efficiency is negligible. The corresponding ratio is calculated with PYTHIA and PHOJET. All the predictions underestimate the measured ratio, as reported in Table 1. The p_t dependence of this ratio is shown in Fig. 5. The Perugia-0, Perugia-11 and D6T tunes systematically underestimate this ratio, while PHOJET correctly reproduces the data for $p_t > 3 \text{ GeV}/c$, and ATLAS-CSC is in agreement with the measurement for $p_t > 1.5 \text{ GeV}/c$.

In order to extract the ω cross section, the ρ and ω contributions must be disentangled, leaving the ρ normalization as an additional free parameter in the fit to the dimuon mass spectrum.

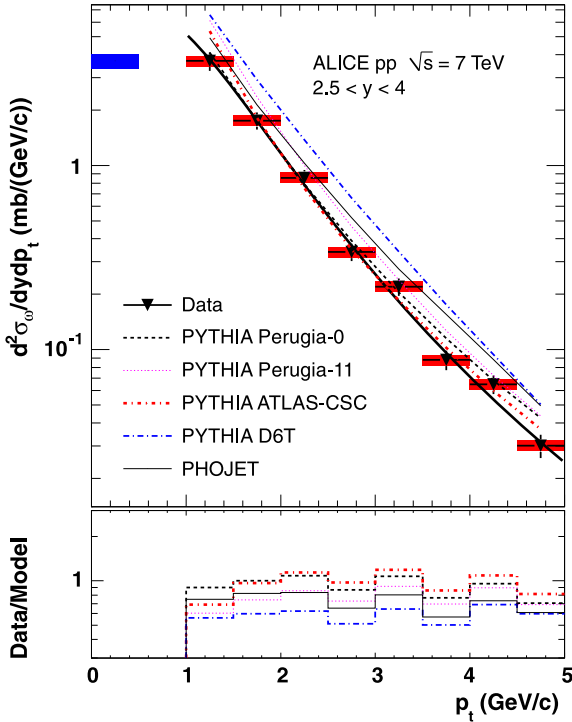


Fig. 6. (Colour online.) Top: Inclusive differential ω production cross section $d^2\sigma_\omega/dy dp_t$ for $2.5 < y < 4$. The error bars represent the quadratic sum of the statistical and systematic uncertainties, the red boxes the point-to-point uncorrelated systematic uncertainty, the blue box on the left the error on normalization. Data are fitted with Eq. (1) (solid line) and compared with the Perugia-0, Perugia-11, ATLAS-CSC and D6T PYTHIA tunes and PHOJET. Bottom: Ratio between data and models.

The result of the fit for $1 < p_t < 5 \text{ GeV}/c$ gives $\sigma_\rho/\sigma_\omega = 1.15 \pm 0.20(\text{stat}) \pm 0.12(\text{syst})$, in agreement with model predictions, as shown in Table 1. The systematic uncertainty was evaluated changing the normalizations of the $\eta' \rightarrow \mu\mu\gamma$ and $\omega \rightarrow \mu\mu\pi^0$ according to the uncertainties in their branching ratios and the background level by $\pm 10\%$, which corresponds to twice the uncertainty in the normalization. The ω production cross section, calculated from this ratio, is $\sigma_\omega(1 < p_t < 5 \text{ GeV}/c, 2.5 < y < 4) = 5.28 \pm 0.54(\text{stat}) \pm 0.49(\text{syst}) \text{ mb}$. This value is in agreement with the Perugia-0 PYTHIA tune, while the other tunes and PHOJET overestimate the ω cross section, as shown in Table 1.

In Fig. 6 (top) the ω differential cross section is shown. Numerical values are reported in Table 2. A fit of Eq. (1) to the data gives $p_0 = 1.44 \pm 0.09 \text{ GeV}/c$ and $n = 3.2 \pm 0.1$. As shown in the same figure (bottom), all the PYTHIA tunes reproduce the p_t slope, while PHOJET gives a slightly harder spectrum.

5. Conclusions

Vector meson production in pp collisions at $\sqrt{s} = 7 \text{ TeV}$ was measured through the dimuon decay channel in $2.5 < y < 4$ and $1 < p_t < 5 \text{ GeV}/c$. The inclusive ϕ production cross section $\sigma_\phi(1 < p_t < 5 \text{ GeV}/c, 2.5 < y < 4) = 0.940 \pm 0.084(\text{stat}) \pm 0.076(\text{syst}) \text{ mb}$ was measured with a sample corresponding to an integrated luminosity $\mathcal{L}_{\text{int}} = 55.7 \text{ nb}^{-1}$. Calculations based on PHOJET and PYTHIA with the ATLAS-CSC and D6T tunes give results that are in agreement with the measurement, while the Perugia-0 and Perugia-11 PYTHIA tunes underestimate the cross section by about a factor of 2 and 1.5, respectively. The ratio $N_\phi/(N_\rho + N_\omega)$, calculated for $1 < p_t < 5 \text{ GeV}/c$, gives $0.416 \pm 0.032 \pm 0.004$. This value is reproduced by PHOJET for $p_t > 3 \text{ GeV}/c$, and by the ATLAS-CSC tune for

$p_t > 1.5 \text{ GeV}/c$, while the other tunes underestimate the ratio in the full range $1 < p_t < 5 \text{ GeV}/c$. By measuring the ratio of the ρ and ω cross sections, $\sigma_\rho/\sigma_\omega = 1.15 \pm 0.20(\text{stat}) \pm 0.12(\text{syst})$, it was possible to extract the inclusive ω production cross section $\sigma_\omega(1 < p_t < 5 \text{ GeV}/c, 2.5 < y < 4) = 5.28 \pm 0.54(\text{stat}) \pm 0.49(\text{syst}) \text{ mb}$. While all models correctly reproduce the measured $\sigma_\rho/\sigma_\omega$ ratio, the ω cross section is correctly reproduced only by the Perugia-0 calculation, and overestimated by the others. The differential production cross sections of ω and ϕ were measured. The p_t dependence of the ϕ cross section agrees well with other measurements done in the kaon decay channel. The ATLAS-CSC and D6T tunes correctly reproduce the ϕ p_t spectrum, while the other calculations predict harder spectra. PHOJET predicts also a slightly harder p_t spectrum for the ω , while PYTHIA provides slopes which are closer to the one obtained with this measurement.

Acknowledgements

The ALICE Collaboration would like to thank all its engineers and technicians for their invaluable contributions to the construction of the experiment and the CERN accelerator teams for the outstanding performance of the LHC complex.

The ALICE Collaboration acknowledges the following funding agencies for their support in building and running the ALICE detector:

Department of Science and Technology, South Africa;
Calouste Gulbenkian Foundation from Lisbon and Swiss Fonds Kidagan, Armenia;
Conselho Nacional de Desenvolvimento Científico e Tecnológico (CNPq), Financiadora de Estudos e Projetos (FINEP), Fundação de Amparo à Pesquisa do Estado de São Paulo (FAPESP);
National Natural Science Foundation of China (NSFC), the Chinese Ministry of Education (CMOE) and the Ministry of Science and Technology of China (MSTC);
Ministry of Education and Youth of the Czech Republic;
Danish Natural Science Research Council, the Carlsberg Foundation and the Danish National Research Foundation;
The European Research Council under the European Community's Seventh Framework Programme;
Helsinki Institute of Physics and the Academy of Finland;
French CNRS-IN2P3, the 'Region Pays de Loire', 'Region Alsace', 'Region Auvergne' and CEA, France;
German BMBF and the Helmholtz Association;
General Secretariat for Research and Technology, Ministry of Development, Greece;
Hungarian OTKA and National Office for Research and Technology (NKTH);
Department of Atomic Energy and Department of Science and Technology of the Government of India;
Istituto Nazionale di Fisica Nucleare (INFN) of Italy;
MEXT Grant-in-Aid for Specially Promoted Research, Japan;
Joint Institute for Nuclear Research, Dubna;
National Research Foundation of Korea (NRF);
CONACYT, DGAPA, México, ALFA-EC and the HELEN Program (High-Energy physics Latin-American-European Network);
Stichting voor Fundamenteel Onderzoek der Materie (FOM) and the Nederlandse Organisatie voor Wetenschappelijk Onderzoek (NWO), Netherlands;
Research Council of Norway (NFR);
Polish Ministry of Science and Higher Education;
National Authority for Scientific Research – NASR (Autoritatea Națională pentru Cercetare Științifică - ANCS);
Federal Agency of Science of the Ministry of Education and Science of Russian Federation, International Science and Technology Center,

Russian Academy of Sciences, Russian Federal Agency of Atomic Energy, Russian Federal Agency for Science and Innovations and CERN-INTAS;
 Ministry of Education of Slovakia;
 CIEMAT, EELA, Ministerio de Educación y Ciencia of Spain, Xunta de Galicia (Consellería de Educación), CEADEN, Cubaenergía, Cuba, and IAEA (International Atomic Energy Agency);
 Swedish Research Council (VR) and Knut & Alice Wallenberg Foundation (KAW);
 Ukraine Ministry of Education and Science;
 United Kingdom Science and Technology Facilities Council (STFC);
 The United States Department of Energy, the United States National Science Foundation, the State of Texas, and the State of Ohio.

Open Access

This article is published Open Access at sciencedirect.com. It is distributed under the terms of the Creative Commons Attribution License 3.0, which permits unrestricted use, distribution, and reproduction in any medium, provided the original authors and source are credited.

References

- [1] T. Sjöstrand, P.Z. Skands, Eur. Phys. J. C 39 (2005) 129.
- [2] K. Aamodt, et al., ALICE Collaboration, Eur. Phys. J. C 71 (2011) 1594.
- [3] T. Sjöstrand, et al., J. High Energy Phys. 0605 (2006) 026.
- [4] R. Engel, Z. Phys. C 66 (1995) 203;
 R. Engel, J. Ranft, Phys. Rev. D 54 (1996) 4244.
- [5] J. Rafelski, B. Müller, Phys. Rev. Lett. 48 (1982) 1066;
 J. Rafelski, B. Müller, Phys. Rev. Lett. 56 (1986) 2334, Erratum.
- [6] A.L.S. Angelis, et al., HELIOS-3 Collaboration, Eur. Phys. J. C 5 (1998) 63.
- [7] C. Alt, et al., NA49 Collaboration, Phys. Rev. Lett. 94 (2005) 052301.
- [8] B. Alessandro, et al., NA50 Collaboration, Phys. Lett. B 555 (2003) 147.
- [9] D. Adamova, et al., CERES Collaboration, Phys. Rev. Lett. 96 (2006) 152301.
- [10] R. Arnaldi, et al., NA60 Collaboration, Eur. Phys. J. C 64 (2009) 1.
- [11] R. Arnaldi, et al., NA60 Collaboration, Phys. Lett. B 699 (2011) 325.
- [12] A. Adare, et al., PHENIX Collaboration, Phys. Rev. C 83 (2011) 024909.
- [13] B.I. Abelev, et al., STAR Collaboration, Phys. Lett. B 673 (2009) 183.
- [14] K. Aamodt, et al., ALICE Collaboration, JINST 3 (2008) S08002.
- [15] M. Gagliardi, et al., ALICE Collaboration, in: Proceedings of the International Workshop on Early Physics with Heavy-Ion Collisions at LHC, July 6th–8th, 2011, Bari, Italy.
- [16] S. van der Meer, ISR-PO/68-31, KEK68-64.
- [17] L. Aphecetche, et al., ALICE Internal Note ALICE-INT-2009-044, <https://edms.cern.ch/document/1054937/1>.
- [18] G. Chabatova, et al., ALICE Internal Note ALICE-INT-2003-002, <https://edms.cern.ch/document/371480/1>.
- [19] P. Braun-Munzinger, P. Crochet, Nucl. Instr. Meth. Phys. Res. A 484 (2002) 564.
- [20] P.Z. Skands, arXiv:0905.3418, 2009.
- [21] I. Abt, et al., HERA-B Collaboration, Eur. Phys. J. C 50 (2007) 315.
- [22] K. Reygers, ALICE Collaboration, J. Phys. G 38 (2011) 124076.
- [23] R. Brun, et al., CERN Program Library Long Write-up, W5013, GEANT3 Detector Description and Simulation Tool, 1994.
- [24] M. Aguilar-Benitez, et al., Z. Phys. C 50 (1991) 405.
- [25] G. Agakichiev, et al., CERES Collaboration, Eur. Phys. J. C 4 (1998) 231.
- [26] A. Uras, et al., NA60 Collaboration, J. Phys. G 38 (2011) 124180.
- [27] M. Schmelling, et al., LHCb Collaboration, CERN-LHCb-CONF-2010-013, <http://cdsweb.cern.ch/record/1311236>, 2010.
- [28] R. Aaij, et al., LHCb Collaboration, Phys. Lett. B 694 (2010) 209.
- [29] K. Nakamura, et al., Particle Data Group, J. Phys. G 37 (2010) 075021.
- [30] K. Aamodt, et al., ALICE Collaboration, Phys. Lett. B 704 (2011) 442.
- [31] G. Anders, et al., CERN-ATS-Note-2011-016 PERF.
- [32] L. Aphecetche, et al., ALICE-SCIENTIFIC-NOTE-2011-001, <http://cdsweb.cern.ch/record/1388921>.
- [33] P. Abreu, et al., DELPHI Collaboration, Phys. Lett. B 406 (1997) 271.
- [34] J.H. Chen, et al., STAR Collaboration, J. Phys. G 35 (2008) 044068.
- [35] P.Z. Skands, Phys. Rev. D 82 (2010) 074018.
- [36] C. Buttar, et al., Acta Phys. Pol. B 35 (2004) 433.
- [37] R. Field, Acta Phys. Pol. B 39 (2008) 2611, arXiv:1003.4220, 2010.
- [38] R. Aaij, et al., LHCb Collaboration, Phys. Lett. B 703 (2011) 267.

ALICE Collaboration

B. Abelev ⁶⁹, A. Abrahantes Quintana ⁶, D. Adamová ⁷⁴, A.M. Adare ¹²⁰, M.M. Aggarwal ⁷⁸, G. Aglieri Rinella ³⁰, A.G. Agocs ⁶⁰, A. Agostinelli ¹⁹, S. Aguilar Salazar ⁵⁶, Z. Ahmed ¹¹⁶, N. Ahmad ¹⁴, A. Ahmad Masoodi ¹⁴, S.U. Ahn ^{64,37}, A. Akindinov ⁴⁶, D. Aleksandrov ⁸⁹, B. Alessandro ⁹⁵, R. Alfaro Molina ⁵⁶, A. Alici ^{96,30,9}, A. Alkin ², E. Almaráz Aviña ⁵⁶, T. Alt ³⁶, V. Altini ^{28,30}, S. Altinpinar ¹⁵, I. Altsybeev ¹¹⁷, C. Andrei ⁷¹, A. Andronic ⁸⁶, V. Anguelov ⁸³, C. Anson ¹⁶, T. Antićić ⁸⁷, F. Antinori ¹⁰⁰, P. Antonioli ⁹⁶, L. Aphecetche ¹⁰², H. Appelshäuser ⁵², N. Arbor ⁶⁵, S. Arcelli ¹⁹, A. Arend ⁵², N. Armesto ¹³, R. Arnaldi ⁹⁵, T. Aronsson ¹²⁰, I.C. Arsene ⁸⁶, M. Arslanbekov ⁵², A. Asryan ¹¹⁷, A. Augustinus ³⁰, R. Averbeck ⁸⁶, T.C. Awes ⁷⁵, J. Äystö ³⁸, M.D. Azmi ¹⁴, M. Bach ³⁶, A. Badalà ⁹⁷, Y.W. Baek ^{64,37}, R. Bailhache ⁵², R. Bala ⁹⁵, R. Baldini Ferroli ⁹, A. Baldissari ¹², A. Baldit ⁶⁴, F. Baltasar Dos Santos Pedrosa ³⁰, J. Bán ⁴⁷, R.C. Baral ⁴⁸, R. Barbera ²⁴, F. Barile ²⁸, G.G. Barnaföldi ⁶⁰, L.S. Barnby ⁹¹, V. Barret ⁶⁴, J. Bartke ¹⁰⁴, M. Basile ¹⁹, N. Bastid ⁶⁴, B. Bathen ⁵⁴, G. Batigne ¹⁰², B. Batyunya ⁵⁹, C. Baumann ⁵², I.G. Bearden ⁷², H. Beck ⁵², I. Belikov ⁵⁸, F. Bellini ¹⁹, R. Bellwied ¹¹⁰, E. Belmont-Moreno ⁵⁶, S. Beole ²⁶, I. Berceanu ⁷¹, A. Bercuci ⁷¹, Y. Berdnikov ⁷⁶, D. Berenyi ⁶⁰, C. Bergmann ⁵⁴, D. Berziano ⁹⁵, L. Betev ³⁰, A. Bhasin ⁸¹, A.K. Bhati ⁷⁸, L. Bianchi ²⁶, N. Bianchi ⁶⁶, C. Bianchin ²², J. Bielčík ³⁴, J. Bielčíková ⁷⁴, A. Bilandžić ⁷³, F. Blanco ¹¹⁰, F. Blanco ⁷, D. Blau ⁸⁹, C. Blume ⁵², M. Boccioli ³⁰, N. Bock ¹⁶, A. Bogdanov ⁷⁰, H. Bøggild ⁷², M. Bogolyubsky ⁴³, L. Boldizsár ⁶⁰, M. Bombara ³⁵, J. Book ⁵², H. Borel ¹², A. Borissov ¹¹⁹, C. Bortolin ^{22,i}, S. Bose ⁹⁰, F. Bossú ^{30,26}, M. Botje ⁷³, S. Böttger ⁵¹, B. Boyer ⁴², P. Braun-Munzinger ⁸⁶, M. Bregant ¹⁰², T. Breitner ⁵¹, M. Broz ³³, R. Brun ³⁰, E. Bruna ^{120,26,95}, G.E. Bruno ²⁸, D. Budnikov ⁸⁸, H. Buesching ⁵², S. Bufalino ^{26,95}, K. Bugaiev ², O. Busch ⁸³, Z. Buthelezi ⁸⁰, D. Caffarri ²², X. Cai ⁴⁰, H. Caines ¹²⁰, E. Calvo Villar ⁹², P. Camerini ²⁰, V. Canoa Roman ^{8,1}, G. Cara Romeo ⁹⁶, W. Carena ³⁰, F. Carena ³⁰, N. Carlin Filho ¹⁰⁷, F. Carminati ³⁰, C.A. Carrillo Montoya ³⁰, A. Casanova Díaz ⁶⁶, M. Caselle ³⁰, J. Castillo Castellanos ¹², J.F. Castillo Hernandez ⁸⁶, E.A.R. Casula ²¹, V. Cataneescu ⁷¹, C. Cavicchioli ³⁰, J. Cepila ³⁴, P. Cerello ⁹⁵, B. Chang ^{38,123}, S. Chapelain ³⁰, J.L. Charvet ¹², S. Chattopadhyay ¹¹⁶, S. Chattopadhyay ⁹⁰, M. Cherney ⁷⁷, C. Cheshkov ^{30,109}, B. Cheynis ¹⁰⁹,

- E. Chiavassa 95, V. Chibante Barroso 30, D.D. Chinellato 108, P. Chochula 30, M. Chojnacki 45,
 P. Christakoglou 73, 45, C.H. Christensen 72, P. Christiansen 29, T. Chujo 114, S.U. Chung 85, C. Cicalo 93,
 L. Cifarelli 19, 30, F. Cindolo 96, J. Cleymans 80, F. Coccetti 9, J.-P. Coffin 58, F. Colamaria 28, D. Colella 28,
 G. Conesa Balbastre 65, Z. Conesa del Valle 30, 58, P. Constantin 83, G. Contin 20, J.G. Contreras 8,
 T.M. Cormier 119, Y. Corrales Morales 26, P. Cortese 27, I. Cortés Maldonado 1, M.R. Cosentino 68, 108,
 F. Costa 30, M.E. Cotallo 7, E. Crescio 8, P. Crochet 64, E. Cruz Alaniz 56, E. Cuautle 55, L. Cunqueiro 66,
 A. Dainese 22, 100, H.H. Dalsgaard 72, A. Danu 50, K. Das 90, D. Das 90, I. Das 90, S. Dash 95, A. Dash 48, 108,
 S. De 116, A. De Azevedo Moregula 66, G.O.V. de Barros 107, A. De Caro 25, 9, G. de Cataldo 94,
 J. de Cuveland 36, A. De Falco 21, *, D. De Gruttola 25, H. Delagrange 102, E. Del Castillo Sanchez 30,
 A. Deloff 101, V. Demanov 88, N. De Marco 95, E. Dénes 60, S. De Pasquale 25, A. Deppman 107,
 G. D Erasmo 28, R. de Rooij 45, D. Di Bari 28, T. Dietel 54, C. Di Giglio 28, S. Di Liberto 99, A. Di Mauro 30,
 P. Di Nezza 66, R. Divià 30, Ø. Djupsland 15, A. Dobrin 119, 29, T. Dobrowolski 101, I. Domínguez 55,
 B. Dönigus 86, O. Dordic 18, O. Driga 102, A.K. Dubey 116, L. Ducroux 109, P. Dupieux 64, A.K. Dutta
 Majumdar 90, M.R. Dutta Majumdar 116, D. Elia 94, D. Emschermann 54, H. Engel 51, H.A. Erdal 32,
 B. Espagnon 42, M. Estienne 102, S. Esumi 114, D. Evans 91, G. Eyyubova 18, D. Fabris 22, 100, J. Faivre 65,
 D. Falchieri 19, A. Fantoni 66, M. Fasel 86, R. Fearick 80, A. Fedunov 59, D. Fehlker 15, L. Feldkamp 54,
 D. Felea 50, G. Feofilov 117, A. Fernández Téllez 1, A. Ferretti 26, R. Ferretti 27, J. Figiel 104,
 M.A.S. Figueiredo 107, S. Filchagin 88, R. Fini 94, D. Finogeev 44, F.M. Fionda 28, E.M. Fiore 28, M. Floris 30,
 S. Foertsch 80, P. Foka 86, S. Fokin 89, E. Fragiocomo 98, M. Fragkiadakis 79, U. Frankenfeld 86, U. Fuchs 30,
 C. Furget 65, M. Fusco Girard 25, J.J. Gaardhøje 72, M. Gagliardi 26, A. Gago 92, M. Gallio 26,
 D.R. Gangadharan 16, P. Ganoti 75, C. Garabatos 86, E. Garcia-Solis 10, I. Garishvili 69, J. Gerhard 36,
 M. Germain 102, C. Geuna 12, M. Gheata 30, A. Gheata 30, B. Ghidini 28, P. Ghosh 116, P. Gianotti 66,
 M.R. Girard 118, P. Giubellino 30, E. Gladysz-Dziadus 104, P. Glässel 83, R. Gomez 106, E.G. Ferreiro 13,
 L.H. González-Trueba 56, P. González-Zamora 7, S. Gorbunov 36, A. Goswami 82, S. Gotovac 103,
 V. Grabski 56, L.K. Graczykowski 118, R. Grajcarek 83, A. Grelli 45, C. Grigoras 30, A. Grigoras 30,
 V. Grigoriev 70, A. Grigoryan 121, S. Grigoryan 59, B. Grinyov 2, N. Grion 98, P. Gros 29,
 J.F. Grosse-Oetringhaus 30, J.-Y. Grossiord 109, R. Grossiord 30, F. Guber 44, R. Guernane 65,
 C. Guerra Gutierrez 92, B. Guerzoni 19, M. Guilbaud 109, K. Gulbrandsen 72, T. Gunji 113, A. Gupta 81,
 R. Gupta 81, H. Gutbrod 86, Ø. Haaland 15, C. Hadjidakis 42, M. Haiduc 50, H. Hamagaki 113, G. Hamar 60,
 B.H. Han 17, L.D. Hanratty 91, A. Hansen 72, Z. Harmanova 35, J.W. Harris 120, M. Hartig 52, D. Hasegan 50,
 D. Hatzifotiadou 96, A. Hayrapetyan 30, 121, M. Heide 54, H. Helstrup 32, A. Herghelegiu 71,
 G. Herrera Corral 8, N. Herrmann 83, K.F. Hetland 32, B. Hicks 120, P.T. Hille 120, B. Hippolyte 58,
 T. Horaguchi 114, Y. Hori 113, P. Hristov 30, I. Hřivnáčová 42, M. Huang 15, S. Huber 86, T.J. Humanic 16,
 D.S. Hwang 17, R. Ichou 64, R. Ilkaev 88, I. Ilkiv 101, M. Inaba 114, E. Incani 21, G.M. Innocenti 26,
 P.G. Innocenti 30, M. Ippolitov 89, M. Irfan 14, C. Ivan 86, M. Ivanov 86, A. Ivanov 117, V. Ivanov 76,
 O. Ivanytskyi 2, A. Jachołkowski 30, P.M. Jacobs 68, L. Jancurová 59, H.J. Jang 63, S. Jangal 58, R. Janik 33,
 M.A. Janik 118, P.H.S.Y. Jayarathna 110, S. Jena 41, R.T. Jimenez Bustamante 55, L. Jirden 30, P.G. Jones 91,
 W. Jung 37, H. Jung 37, A. Jusko 91, A.B. Kaidalov 46, V. Kakoyan 121, S. Kalcher 36, P. Kaliňák 47,
 M. Kalisky 54, T. Kalliokoski 38, A. Kalweit 53, K. Kanaki 15, J.H. Kang 123, V. Kaplin 70, A. Karasu
 Uysal 30, 122, O. Karavichev 44, T. Karavicheva 44, E. Karpechev 44, A. Kazantsev 89, U. Kebschull 62, 51,
 R. Keidel 124, M.M. Khan 14, P. Khan 90, S.A. Khan 116, A. Khanzadeev 76, Y. Kharlov 43, B. Kileng 32,
 D.W. Kim 37, M. Kim 123, J.H. Kim 17, S.H. Kim 37, S. Kim 17, B. Kim 123, T. Kim 123, D.J. Kim 38, J.S. Kim 37,
 S. Kirsch 36, 30, I. Kisiel 36, S. Kiselev 46, A. Kisiel 30, 118, J.L. Klay 4, J. Klein 83, C. Klein-Bösing 54,
 M. Kliemant 52, A. Kluge 30, M.L. Knichel 86, K. Koch 83, M.K. Köhler 86, A. Kolojvari 117, V. Kondratiev 117,
 N. Kondratyeva 70, A. Konevskikh 44, A. Korneev 88, C. Kottachchi Kankamge Don 119, R. Kour 91,
 M. Kowalski 104, S. Kox 65, G. Koyithatta Meethaleveedu 41, J. Kral 38, I. Králik 47, F. Kramer 52, I. Kraus 86,
 T. Krawutschke 83, 31, M. Kretz 36, M. Krivda 91, 47, F. Krizek 38, M. Krus 34, E. Kryshen 76, M. Krzewicki 73, 86,
 Y. Kucherlaev 89, C. Kuhn 58, P.G. Kuijer 73, P. Kurashvili 101, A.B. Kurepin 44, A. Kurepin 44, A. Kuryakin 88,
 V. Kushpil 74, S. Kushpil 74, H. Kvaerno 18, M.J. Kweon 83, Y. Kwon 123, P. Ladrón de Guevara 55,
 I. Lakomov 117, R. Langoy 15, C. Lara 51, A. Lardeux 102, P. La Rocca 24, C. Lazzeroni 91, R. Lea 20,
 Y. Le Bornec 42, K.S. Lee 37, S.C. Lee 37, F. Lefèvre 102, J. Lehnert 52, L. Leistam 30, M. Lenhardt 102,
 V. Lenti 94, H. León 56, I. León Monzón 106, H. León Vargas 52, P. Lévai 60, X. Li 11, J. Lien 15, R. Lietava 91,

- S. Lindal ¹⁸, V. Lindenstruth ³⁶, C. Lippmann ^{86,30}, M.A. Lisa ¹⁶, L. Liu ¹⁵, P.I. Loenne ¹⁵, V.R. Loggins ¹¹⁹, V. Loginov ⁷⁰, S. Lohn ³⁰, D. Lohner ⁸³, C. Loizides ⁶⁸, K.K. Loo ³⁸, X. Lopez ⁶⁴, E. López Torres ⁶, G. Løvhøiden ¹⁸, X.-G. Lu ⁸³, P. Luettig ⁵², M. Lunardon ²², J. Luo ⁴⁰, G. Luparello ⁴⁵, L. Luquin ¹⁰², C. Luzzi ³⁰, R. Ma ¹²⁰, K. Ma ⁴⁰, D.M. Madagodahettige-Don ¹¹⁰, A. Maevkaya ⁴⁴, M. Mager ^{53,30}, D.P. Mahapatra ⁴⁸, A. Maire ⁵⁸, M. Malaev ⁷⁶, I. Maldonado Cervantes ⁵⁵, L. Malinina ^{59,ii}, D. Mal'Kevich ⁴⁶, P. Malzacher ⁸⁶, A. Mamontov ⁸⁸, L. Manceau ⁹⁵, L. Mangotra ⁸¹, V. Manko ⁸⁹, F. Manso ⁶⁴, V. Manzari ⁹⁴, Y. Mao ^{65,40}, M. Marchisone ^{64,26}, J. Mareš ⁴⁹, G.V. Margagliotti ^{20,98}, A. Margotti ⁹⁶, A. Marín ⁸⁶, C. Markert ¹⁰⁵, I. Martashvili ¹¹², P. Martinengo ³⁰, M.I. Martínez ¹, A. Martínez Davalos ⁵⁶, G. Martínez García ¹⁰², Y. Martynov ², A. Mas ¹⁰², S. Masciocchi ⁸⁶, M. Masera ²⁶, A. Masoni ⁹³, L. Massacrier ¹⁰⁹, M. Mastromarco ⁹⁴, A. Mastroserio ^{28,30}, Z.L. Matthews ⁹¹, A. Matyja ¹⁰², D. Mayani ⁵⁵, C. Mayer ¹⁰⁴, J. Mazer ¹¹², M.A. Mazzoni ⁹⁹, F. Meddi ²³, A. Menchaca-Rocha ⁵⁶, J. Mercado Pérez ⁸³, M. Meres ³³, Y. Miake ¹¹⁴, A. Michalon ⁵⁸, J. Midori ³⁹, L. Milano ²⁶, J. Milosevic ^{18,iii}, A. Mischke ⁴⁵, A.N. Mishra ⁸², D. Miśkowiec ^{86,30}, C. Mitu ⁵⁰, J. Mlynarz ¹¹⁹, A.K. Mohanty ³⁰, B. Mohanty ¹¹⁶, L. Molnar ³⁰, L. Montaño Zetina ⁸, M. Monteno ⁹⁵, E. Montes ⁷, T. Moon ¹²³, M. Morando ²², D.A. Moreira De Godoy ¹⁰⁷, S. Moretto ²², A. Morsch ³⁰, V. Muccifora ⁶⁶, E. Mudnic ¹⁰³, S. Muhuri ¹¹⁶, H. Müller ³⁰, M.G. Munhoz ¹⁰⁷, L. Musa ³⁰, A. Musso ⁹⁵, B.K. Nandi ⁴¹, R. Nania ⁹⁶, E. Nappi ⁹⁴, C. Natrass ¹¹², N.P. Naumov ⁸⁸, S. Navin ⁹¹, T.K. Nayak ¹¹⁶, S. Nazarenko ⁸⁸, G. Nazarov ⁸⁸, A. Nedosekin ⁴⁶, M. Nicassio ²⁸, B.S. Nielsen ⁷², T. Niida ¹¹⁴, S. Nikolaev ⁸⁹, V. Nikolic ⁸⁷, S. Nikulin ⁸⁹, V. Nikulin ⁷⁶, B.S. Nilsen ⁷⁷, M.S. Nilsson ¹⁸, F. Noferini ^{96,9}, P. Nomokonov ⁵⁹, G. Nooren ⁴⁵, N. Novitzky ³⁸, A. Nyanin ⁸⁹, A. Nyatha ⁴¹, C. Nygaard ⁷², J. Nystrand ¹⁵, H. Obayashi ³⁹, A. Ochiroy ¹¹⁷, H. Oeschler ^{53,30}, S.K. Oh ³⁷, S. Oh ¹²⁰, J. Oleniacz ¹¹⁸, C. Oppedisano ⁹⁵, A. Ortiz Velasquez ⁵⁵, G. Ortona ^{30,26}, A. Oskarsson ²⁹, P. Ostrowski ¹¹⁸, I. Otterlund ²⁹, J. Otwinowski ⁸⁶, K. Oyama ⁸³, K. Ozawa ¹¹³, Y. Pachmayer ⁸³, M. Pachr ³⁴, F. Padilla ²⁶, P. Pagano ²⁵, G. Paić ⁵⁵, F. Painke ³⁶, C. Pajares ¹³, S. Pal ¹², S.K. Pal ¹¹⁶, A. Palaha ⁹¹, A. Palmeri ⁹⁷, V. Papikyan ¹²¹, G.S. Pappalardo ⁹⁷, W.J. Park ⁸⁶, A. Passfeld ⁵⁴, B. Pastirčák ⁴⁷, D.I. Patalakha ⁴³, V. Paticchio ⁹⁴, A. Pavlinov ¹¹⁹, T. Pawlak ¹¹⁸, T. Peitzmann ⁴⁵, M. Perales ¹⁰, E. Pereira De Oliveira Filho ¹⁰⁷, D. Peresunko ⁸⁹, C.E. Pérez Lara ⁷³, E. Perez Lezama ⁵⁵, D. Perini ³⁰, D. Perrino ²⁸, W. Peryt ¹¹⁸, A. Pesci ⁹⁶, V. Peskov ^{30,55}, Y. Pestov ³, V. Petráček ³⁴, M. Petran ³⁴, M. Petris ⁷¹, P. Petrov ⁹¹, M. Petrovici ⁷¹, C. Petta ²⁴, S. Piano ⁹⁸, A. Piccotti ⁹⁵, M. Pikna ³³, P. Pillot ¹⁰², O. Pinazza ³⁰, L. Pinsky ¹¹⁰, N. Pitz ⁵², F. Piuz ³⁰, D.B. Piyarathna ¹¹⁰, M. Płoskoń ⁶⁸, J. Pluta ¹¹⁸, T. Pocheptsov ^{59,18}, S. Pochybova ⁶⁰, P.L.M. Podesta-Lerma ¹⁰⁶, M.G. Poghosyan ^{30,26}, K. Polák ⁴⁹, B. Polichtchouk ⁴³, A. Pop ⁷¹, S. Porteboeuf-Houssais ⁶⁴, V. Pospíšil ³⁴, B. Potukuchi ⁸¹, S.K. Prasad ¹¹⁹, R. Preghenella ^{96,9}, F. Prino ⁹⁵, C.A. Pruneau ¹¹⁹, I. Pschenichnov ⁴⁴, S. Puchagin ⁸⁸, G. Puddu ²¹, A. Pulvirenti ^{24,30}, V. Punin ⁸⁸, M. Putiš ³⁵, J. Putschke ^{119,120}, E. Quercigh ³⁰, H. Qvigstad ¹⁸, A. Rachevski ⁹⁸, A. Rademakers ³⁰, S. Radomski ⁸³, T.S. Räihä ³⁸, J. Rak ³⁸, A. Rakotozafindrabe ¹², L. Ramello ²⁷, A. Ramírez Reyes ⁸, R. Raniwala ⁸², S. Raniwala ⁸², S.S. Räsänen ³⁸, B.T. Rascanu ⁵², D. Rathee ⁷⁸, K.F. Read ¹¹², J.S. Real ⁶⁵, K. Redlich ^{101,57}, P. Reichelt ⁵², M. Reicher ⁴⁵, R. Renfordt ⁵², A.R. Reolon ⁶⁶, A. Reshetin ⁴⁴, F. Rettig ³⁶, J.-P. Revol ³⁰, K. Reygers ⁸³, L. Riccati ⁹⁵, R.A. Ricci ⁶⁷, M. Richter ¹⁸, P. Riedler ³⁰, W. Riegler ³⁰, F. Riggi ^{24,97}, M. Rodríguez Cahuantzi ¹, D. Rohr ³⁶, D. Röhrich ¹⁵, R. Romita ⁸⁶, F. Ronchetti ⁶⁶, P. Rosnet ⁶⁴, S. Rossegger ³⁰, A. Rossi ²², F. Roukoutakis ⁷⁹, C. Roy ⁵⁸, P. Roy ⁹⁰, A.J. Rubio Montero ⁷, R. Rui ²⁰, E. Ryabinkin ⁸⁹, A. Rybicki ¹⁰⁴, S. Sadovsky ⁴³, K. Šafařík ³⁰, P.K. Sahu ⁴⁸, J. Saini ¹¹⁶, H. Sakaguchi ³⁹, S. Sakai ⁶⁸, D. Sakata ¹¹⁴, C.A. Salgado ¹³, S. Sambyal ⁸¹, V. Samsonov ⁷⁶, X. Sanchez Castro ⁵⁵, L. Šándor ⁴⁷, A. Sandoval ⁵⁶, M. Sano ¹¹⁴, S. Sano ¹¹³, R. Santo ⁵⁴, R. Santoro ^{94,30}, J. Sarkamo ³⁸, E. Scapparone ⁹⁶, F. Scarlassara ²², R.P. Scharenberg ⁸⁴, C. Schiaua ⁷¹, R. Schicker ⁸³, C. Schmidt ⁸⁶, H.R. Schmidt ^{86,115}, S. Schreiner ³⁰, S. Schuchmann ⁵², J. Schukraft ³⁰, Y. Schutz ^{30,102}, K. Schwarz ⁸⁶, K. Schweda ^{86,83}, G. Scioli ¹⁹, E. Scomparin ⁹⁵, P.A. Scott ⁹¹, R. Scott ¹¹², G. Segato ²², I. Selyuzhenkov ⁸⁶, S. Senyukov ^{27,58}, J. Seo ⁸⁵, S. Serci ²¹, E. Serradilla ^{7,56}, A. Sevcenco ⁵⁰, I. Sgura ⁹⁴, A. Shabetai ¹⁰², G. Shabratova ⁵⁹, R. Shahoyan ³⁰, N. Sharma ⁷⁸, S. Sharma ⁸¹, K. Shigaki ³⁹, M. Shimomura ¹¹⁴, K. Shtejer ⁶, Y. Sibiriak ⁸⁹, M. Siciliano ²⁶, E. Sicking ³⁰, S. Siddhanta ⁹³, T. Siemianczuk ¹⁰¹, D. Silvermyr ⁷⁵, G. Simonetti ^{28,30}, R. Singaraju ¹¹⁶, R. Singh ⁸¹, S. Singha ¹¹⁶, B.C. Sinha ¹¹⁶, T. Sinha ⁹⁰, B. Sitar ³³, M. Sitta ²⁷, T.B. Skaali ¹⁸, K. Skjerdal ¹⁵, R. Smakal ³⁴, N. Smirnov ¹²⁰, R. Snellings ⁴⁵, C. Søgaard ⁷², R. Soltz ⁶⁹, H. Son ¹⁷, M. Song ¹²³, J. Song ⁸⁵, C. Soos ³⁰, F. Soramel ²², I. Sputowska ¹⁰⁴, M. Spyropoulou-Stassinaki ⁷⁹, B.K. Srivastava ⁸⁴, J. Stachel ⁸³, I. Stan ⁵⁰, I. Stan ⁵⁰, G. Stefanek ¹⁰¹, G. Stefanini ³⁰, T. Steinbeck ³⁶, M. Steinpreis ¹⁶, E. Stenlund ²⁹, G. Steyn ⁸⁰, D. Stocco ¹⁰²,

M. Stolpovskiy ⁴³, K. Strabykin ⁸⁸, P. Strmen ³³, A.A.P. Suaide ¹⁰⁷, M.A. Subieta Vásquez ²⁶, T. Sugitate ³⁹, C. Suire ⁴², M. Sukhorukov ⁸⁸, R. Sultanov ⁴⁶, M. Šumbera ⁷⁴, T. Susa ⁸⁷, A. Szanto de Toledo ¹⁰⁷, I. Szarka ³³, A. Szostak ¹⁵, C. Tagridis ⁷⁹, J. Takahashi ¹⁰⁸, J.D. Tapia Takaki ⁴², A. Tauro ³⁰, G. Tejeda Muñoz ¹, A. Telesca ³⁰, C. Terrevoli ²⁸, J. Thäder ⁸⁶, D. Thomas ⁴⁵, J.H. Thomas ⁸⁶, R. Tieulent ¹⁰⁹, A.R. Timmins ¹¹⁰, D. Tlusty ³⁴, A. Toia ^{36,30}, H. Torii ^{39,113}, L. Toscano ⁹⁵, F. Tosello ⁹⁵, T. Traczyk ¹¹⁸, D. Truesdale ¹⁶, W.H. Trzaska ³⁸, T. Tsuji ¹¹³, A. Tumkin ⁸⁸, R. Turrisi ¹⁰⁰, T.S. Tveter ¹⁸, J. Ulery ⁵², K. Ullaland ¹⁵, J. Ulrich ^{62,51}, A. Uras ¹⁰⁹, J. Urbán ³⁵, G.M. Urciuoli ⁹⁹, G.L. Usai ²¹, M. Vajzer ^{34,74}, M. Vala ^{59,47}, L. Valencia Palomo ⁴², S. Vallero ⁸³, N. van der Kolk ⁷³, P. Vande Vyvre ³⁰, M. van Leeuwen ⁴⁵, L. Vannucci ⁶⁷, A. Vargas ¹, R. Varma ⁴¹, M. Vasileiou ⁷⁹, A. Vasiliev ⁸⁹, V. Vechernin ¹¹⁷, M. Veldhoen ⁴⁵, M. Venaruzzo ²⁰, E. Vercellin ²⁶, S. Vergara ¹, D.C. Vernekohl ⁵⁴, R. Vernet ⁵, M. Verweij ⁴⁵, L. Vickovic ¹⁰³, G. Viesti ²², O. Vikhlyantsev ⁸⁸, Z. Vilakazi ⁸⁰, O. Villalobos Baillie ⁹¹, L. Vinogradov ¹¹⁷, A. Vinogradov ⁸⁹, Y. Vinogradov ⁸⁸, T. Virgili ²⁵, Y.P. Viyogi ¹¹⁶, A. Vodopyanov ⁵⁹, S. Voloshin ¹¹⁹, K. Voloshin ⁴⁶, G. Volpe ^{28,30}, B. von Haller ³⁰, D. Vranic ⁸⁶, G. Øvrebekk ¹⁵, J. Vrláková ³⁵, B. Vulpescu ⁶⁴, A. Vyushin ⁸⁸, V. Wagner ³⁴, B. Wagner ¹⁵, R. Wan ^{58,40}, Y. Wang ⁸³, M. Wang ⁴⁰, Y. Wang ⁴⁰, D. Wang ⁴⁰, K. Watanabe ¹¹⁴, J.P. Wessels ^{30,54}, U. Westerhoff ⁵⁴, J. Wiechula ^{83,115}, J. Wikne ¹⁸, M. Wilde ⁵⁴, A. Wilk ⁵⁴, G. Wilk ¹⁰¹, M.C.S. Williams ⁹⁶, B. Windelband ⁸³, L. Xaplanteris Karampatsos ¹⁰⁵, S. Yang ¹⁵, H. Yang ¹², S. Yano ³⁹, S. Yasnopolskiy ⁸⁹, J. Yi ⁸⁵, Z. Yin ⁴⁰, H. Yokoyama ¹¹⁴, I.-K. Yoo ⁸⁵, J. Yoon ¹²³, W. Yu ⁵², X. Yuan ⁴⁰, I. Yushmanov ⁸⁹, C. Zach ³⁴, C. Zampolli ^{96,30}, S. Zaporozhets ⁵⁹, A. Zarochentsev ¹¹⁷, P. Závada ⁴⁹, N. Zaviyalov ⁸⁸, H. Zbroszczyk ¹¹⁸, P. Zelnicek ^{30,51}, I. Zgura ⁵⁰, M. Zhalov ⁷⁶, X. Zhang ^{64,40}, D. Zhou ⁴⁰, Y. Zhou ⁴⁵, F. Zhou ⁴⁰, X. Zhu ⁴⁰, A. Zichichi ^{19,9}, A. Zimmermann ⁸³, G. Zinovjev ², Y. Zoccarato ¹⁰⁹, M. Zynovyev ²

¹ Benemérita Universidad Autónoma de Puebla, Puebla, Mexico² Bogolyubov Institute for Theoretical Physics, Kiev, Ukraine³ Budker Institute for Nuclear Physics, Novosibirsk, Russia⁴ California Polytechnic State University, San Luis Obispo, CA, United States⁵ Centre de Calcul de l'IN2P3, Villeurbanne, France⁶ Centro de Aplicaciones Tecnológicas y Desarrollo Nuclear (CEADEN), Havana, Cuba⁷ Centro de Investigaciones Energéticas Medioambientales y Tecnológicas (CIEMAT), Madrid, Spain⁸ Centro de Investigación y de Estudios Avanzados (CINVESTAV), Mexico City and Mérida, Mexico⁹ Centro Fermi – Centro Studi e Ricerche e Museo Storico della Fisica "Enrico Fermi", Rome, Italy¹⁰ Chicago State University, Chicago, IL, United States¹¹ China Institute of Atomic Energy, Beijing, China¹² Commissariat à l'Energie Atomique, IRFU, Saclay, France¹³ Departamento de Física de Partículas and IGFAE, Universidad de Santiago de Compostela, Santiago de Compostela, Spain¹⁴ Department of Physics, Aligarh Muslim University, Aligarh, India¹⁵ Department of Physics and Technology, University of Bergen, Bergen, Norway¹⁶ Department of Physics, Ohio State University, Columbus, OH, United States¹⁷ Department of Physics, Sejong University, Seoul, South Korea¹⁸ Department of Physics, University of Oslo, Oslo, Norway¹⁹ Dipartimento di Fisica dell'Università and Sezione INFN, Bologna, Italy²⁰ Dipartimento di Fisica dell'Università and Sezione INFN, Trieste, Italy²¹ Dipartimento di Fisica dell'Università and Sezione INFN, Cagliari, Italy²² Dipartimento di Fisica dell'Università and Sezione INFN, Padova, Italy²³ Dipartimento di Fisica dell'Università 'La Sapienza' and Sezione INFN, Rome, Italy²⁴ Dipartimento di Fisica e Astronomia dell'Università and Sezione INFN, Catania, Italy²⁵ Dipartimento di Fisica 'E.R. Caianiello' dell'Università and Gruppo Collegato INFN, Salerno, Italy²⁶ Dipartimento di Fisica Sperimentale dell'Università and Sezione INFN, Turin, Italy²⁷ Dipartimento di Scienze e Tecnologie Avanzate dell'Università del Piemonte Orientale and Gruppo Collegato INFN, Alessandria, Italy²⁸ Dipartimento Interateneo di Fisica 'M. Merlin' and Sezione INFN, Bari, Italy²⁹ Division of Experimental High Energy Physics, University of Lund, Lund, Sweden³⁰ European Organization for Nuclear Research (CERN), Geneva, Switzerland³¹ Fachhochschule Köln, Köln, Germany³² Faculty of Engineering, Bergen University College, Bergen, Norway³³ Faculty of Mathematics, Physics and Informatics, Comenius University, Bratislava, Slovakia³⁴ Faculty of Nuclear Sciences and Physical Engineering, Czech Technical University in Prague, Prague, Czech Republic³⁵ Faculty of Science, P.J. Šafárik University, Košice, Slovakia³⁶ Frankfurt Institute for Advanced Studies, Johann Wolfgang Goethe-Universität Frankfurt, Frankfurt, Germany³⁷ Gangneung-Wonju National University, Gangneung, South Korea³⁸ Helsinki Institute of Physics (HIP) and University of Jyväskylä, Jyväskylä, Finland³⁹ Hiroshima University, Hiroshima, Japan⁴⁰ Hua-Zhong Normal University, Wuhan, China⁴¹ Indian Institute of Technology, Mumbai, India⁴² Institut de Physique Nucléaire d'Orsay (IPNO), Université Paris-Sud, CNRS-IN2P3, Orsay, France⁴³ Institute for High Energy Physics, Protvino, Russia⁴⁴ Institute for Nuclear Research, Academy of Sciences, Moscow, Russia⁴⁵ Nikhef, National Institute for Subatomic Physics and Institute for Subatomic Physics of Utrecht University, Utrecht, Netherlands⁴⁶ Institute for Theoretical and Experimental Physics, Moscow, Russia

- ⁴⁷ Institute of Experimental Physics, Slovak Academy of Sciences, Košice, Slovakia
⁴⁸ Institute of Physics, Bhubaneswar, India
⁴⁹ Institute of Physics, Academy of Sciences of the Czech Republic, Prague, Czech Republic
⁵⁰ Institute of Space Sciences (ISS), Bucharest, Romania
⁵¹ Institut für Informatik, Johann Wolfgang Goethe-Universität Frankfurt, Frankfurt, Germany
⁵² Institut für Kernphysik, Johann Wolfgang Goethe-Universität Frankfurt, Frankfurt, Germany
⁵³ Institut für Kernphysik, Technische Universität Darmstadt, Darmstadt, Germany
⁵⁴ Institut für Kernphysik, Westfälische Wilhelms-Universität Münster, Münster, Germany
⁵⁵ Instituto de Ciencias Nucleares, Universidad Nacional Autónoma de México, Mexico City, Mexico
⁵⁶ Instituto de Física, Universidad Nacional Autónoma de México, Mexico City, Mexico
⁵⁷ Institut of Theoretical Physics, University of Wrocław, Poland
⁵⁸ Institut Pluridisciplinaire Hubert Curien (IPHC), Université de Strasbourg, CNRS-IN2P3, Strasbourg, France
⁵⁹ Joint Institute for Nuclear Research (JINR), Dubna, Russia
⁶⁰ KFKI Research Institute for Particle and Nuclear Physics, Hungarian Academy of Sciences, Budapest, Hungary
⁶¹ Kharkiv Institute of Physics and Technology (KIPT), National Academy of Sciences of Ukraine (NASU), Kharkov, Ukraine
⁶² Kirchhoff-Institut für Physik, Ruprecht-Karls-Universität Heidelberg, Heidelberg, Germany
⁶³ Korea Institute of Science and Technology Information, South Korea
⁶⁴ Laboratoire de Physique Corpusculaire (LPC), Clermont Université, Université Blaise Pascal, CNRS-IN2P3, Clermont-Ferrand, France
⁶⁵ Laboratoire de Physique Subatomique et de Cosmologie (LPSC), Université Joseph Fourier, CNRS-IN2P3, Institut Polytechnique de Grenoble, Grenoble, France
⁶⁶ Laboratori Nazionali di Frascati, INFN, Frascati, Italy
⁶⁷ Laboratori Nazionali di Legnaro, INFN, Legnaro, Italy
⁶⁸ Lawrence Berkeley National Laboratory, Berkeley, CA, United States
⁶⁹ Lawrence Livermore National Laboratory, Livermore, CA, United States
⁷⁰ Moscow Engineering Physics Institute, Moscow, Russia
⁷¹ National Institute for Physics and Nuclear Engineering, Bucharest, Romania
⁷² Niels Bohr Institute, University of Copenhagen, Copenhagen, Denmark
⁷³ Nikhef, National Institute for Subatomic Physics, Amsterdam, Netherlands
⁷⁴ Nuclear Physics Institute, Academy of Sciences of the Czech Republic, Řež u Prahy, Czech Republic
⁷⁵ Oak Ridge National Laboratory, Oak Ridge, TN, United States
⁷⁶ Petersburg Nuclear Physics Institute, Gatchina, Russia
⁷⁷ Physics Department, Creighton University, Omaha, NE, United States
⁷⁸ Physics Department, Panjab University, Chandigarh, India
⁷⁹ Physics Department, University of Athens, Athens, Greece
⁸⁰ Physics Department, University of Cape Town, iThemba LABS, Cape Town, South Africa
⁸¹ Physics Department, University of Jammu, Jammu, India
⁸² Physics Department, University of Rajasthan, Jaipur, India
⁸³ Physikalisches Institut, Ruprecht-Karls-Universität Heidelberg, Heidelberg, Germany
⁸⁴ Purdue University, West Lafayette, IN, United States
⁸⁵ Pusan National University, Pusan, South Korea
⁸⁶ Research Division and ExtreMe Matter Institute EMMI, GSI Helmholtzzentrum für Schwerionenforschung, Darmstadt, Germany
⁸⁷ Rudjer Bošković Institute, Zagreb, Croatia
⁸⁸ Russian Federal Nuclear Center (VNIIEF), Sarov, Russia
⁸⁹ Russian Research Centre Kurchatov Institute, Moscow, Russia
⁹⁰ Saha Institute of Nuclear Physics, Kolkata, India
⁹¹ School of Physics and Astronomy, University of Birmingham, Birmingham, United Kingdom
⁹² Sección Física, Departamento de Ciencias, Pontificia Universidad Católica del Perú, Lima, Peru
⁹³ Sezione INFN, Cagliari, Italy
⁹⁴ Sezione INFN, Bari, Italy
⁹⁵ Sezione INFN, Turin, Italy
⁹⁶ Sezione INFN, Bologna, Italy
⁹⁷ Sezione INFN, Catania, Italy
⁹⁸ Sezione INFN, Trieste, Italy
⁹⁹ Sezione INFN, Rome, Italy
¹⁰⁰ Sezione INFN, Padova, Italy
¹⁰¹ Soltan Institute for Nuclear Studies, Warsaw, Poland
¹⁰² SUBATECH, Ecole des Mines de Nantes, Université de Nantes, CNRS-IN2P3, Nantes, France
¹⁰³ Technical University of Split FESB, Split, Croatia
¹⁰⁴ The Henryk Niewodniczanski Institute of Nuclear Physics, Polish Academy of Sciences, Cracow, Poland
¹⁰⁵ The University of Texas at Austin, Physics Department, Austin, TX, United States
¹⁰⁶ Universidad Autónoma de Sinaloa, Culiacán, Mexico
¹⁰⁷ Universidade de São Paulo (USP), São Paulo, Brazil
¹⁰⁸ Universidade Estadual de Campinas (UNICAMP), Campinas, Brazil
¹⁰⁹ Université de Lyon, Université Lyon 1, CNRS/IN2P3, IPN-Lyon, Villeurbanne, France
¹¹⁰ University of Houston, Houston, TX, United States
¹¹¹ University of Technology and Austrian Academy of Sciences, Vienna, Austria
¹¹² University of Tennessee, Knoxville, TN, United States
¹¹³ University of Tokyo, Tokyo, Japan
¹¹⁴ University of Tsukuba, Tsukuba, Japan
¹¹⁵ Eberhard Karls Universität Tübingen, Tübingen, Germany
¹¹⁶ Variable Energy Cyclotron Centre, Kolkata, India
¹¹⁷ V. Fock Institute for Physics, St. Petersburg State University, St. Petersburg, Russia
¹¹⁸ Warsaw University of Technology, Warsaw, Poland
¹¹⁹ Wayne State University, Detroit, MI, United States
¹²⁰ Yale University, New Haven, CT, United States
¹²¹ Yerevan Physics Institute, Yerevan, Armenia
¹²² Yildiz Technical University, Istanbul, Turkey
¹²³ Yonsei University, Seoul, South Korea
¹²⁴ Zentrum für Technologietransfer und Telekommunikation (ZTT), Fachhochschule Worms, Worms, Germany

* Corresponding author.

E-mail address: alessandro.de.falco@ca.infn.it (A. De Falco).

ⁱ Also at: Dipartimento di Fisica dell'Università, Udine, Italy.

ⁱⁱ Also at: M.V. Lomonosov Moscow State University, D.V. Skobeltsyn Institute of Nuclear Physics, Moscow, Russia.

ⁱⁱⁱ Also at: "Vinča" Institute of Nuclear Sciences, Belgrade, Serbia.